

Estimating Tidal Effects in Spring Discharge: A Multiscale Method Using Correlated Phenomena

Eric Chicken*

Department of Statistics
Florida State University
Tallahassee, FL 32306

David E. Loper

Geophysical Fluid Dynamics Institute
Florida State University
Tallahassee, FL 32306

Christopher L. Werner

Geophysical Fluid Dynamics Institute
Florida State University
Tallahassee, FL 32306

Abstract

A new method is proposed to remove accurately one signal's influence from another. In particular, tidal influence on discharge from a natural artesian spring in the Woodville Karst Plain is quantified and is separated from that portion of the discharge due to other factors such as rainfall. Statistical correlation between the signals is used as a thresholding parameter in this new wavelet method. Variants of the estimator are developed for differing assumptions on the relations of the signals. This new method is shown to be effective at identifying and separating tidal signals, both regular (luni-solar forcing) and irregular (storms and hurricanes), from the discharge signal.

1 Introduction

Modeling groundwater flow within a coastal karst aquifer is a difficult task, in large part due to the multitude of factors, including rainfall, sinking streams, luni-solar tides and storm tides, that can affect the magnitude of discharge from the aquifer, particularly at springs. A primary goal of modeling efforts is the accurate simulation of discharge due to rainfall and sinking streams. A necessary preliminary step is to remove from the discharge measurements that portion resulting from the influence of tides. The purpose of this paper is to describe a procedure to accomplish this step.

This paper was motivated by a desire to separate tidal influence from the discharge measured at Wakulla Springs, a large spring in north central Florida. The Florida

*Corresponding author: email chicken@stat.fsu.edu

hurricane season of 2004 demonstrated that tide greatly affects the discharge at this spring, see Loper et al. (2005). Although the procedure described below will be developed in the context of this specific example, it has general applicability.

Existing methods are not well suited to separate the tidal and non-tidal portions of the discharge. For example, Fourier analysis is inappropriate because storm activity causes the tidal signal for the region to be irregular. Due to this irregularity, an estimation technique is needed that is localized in time. Fourier analysis is not well localized. Various function smoothing techniques, kernel smoothing, for example, also give poor results. A smoother can be tuned via bandwidth selection, kernel choice, etc., to identify and remove tidal effects at a certain resolution, but it could not do the same for tidal effects at a different scale, such as the storm tide found during hurricane events. To overcome these difficulties presented by our data, we turn to wavelet analyses.

Wavelets have been used to examine regular effects in signals. For example, the continuous wavelet transform is well-suited for identifying frequencies within a signal (Vidakovic (1995)). Labat et al. (2000) used wavelet analysis to identify periodic components of a signal by smoothing with thresholding. They also identified common frequencies and features between two signals via wavelets. However, they did not consider the removal of the influence of one signal from another. Other uses of wavelets with respect to hydrology include Gan (2001) and Lim and Lye (2004).

In this paper, we present a new method for determining the tidal influence on the discharge. The method uses simultaneous multiscale wavelet analysis of two signals (in our case, tide and discharge) to recover a third signal (non-tidal component of discharge). This is done by thresholding the wavelets in a new manner based on the statistical concept of correlation.

As noted above, our method is described in the context of groundwater discharge at a large inland spring and tides, but extends to a wide variety of signal separation situations. We will present conditions in which this method is valid.

We discuss the estimator in Section 2. Section 3 applies the estimator to two cases: a simple case, in which the tidal component to be removed is very regular, and a second, more complex case involving both regular tides and tides induced by the passage of two hurricanes.

2 The Estimator

Suppose that a function is of the form

$$f(x_i) = g(x_i) + h(x_i), \quad i = 1, 2, \dots, n \quad (1)$$

where f is observed, but g and h are not. The goal is to estimate g . To do so, we must estimate and remove the function h from f . In general, this cannot be done unless we know some additional information about the function h . For example, if h is random error then (1) reduces to the case of nonparametric regression and is easily solved for a variety of situations.

The function h is caused by an external process that also produces a known function, h' . Although the form of the relation between h and h' is not known, we will assume that the temporal variation of the two are identical, or nearly so. In the present example, f is the observed discharge at Wakulla Springs and h' is the tide measured by a nearby coastal tide gauge.

The remainder of this section describes the relation between h and h' , gives a general background on wavelets and multiresolution analysis and provides the specific form of the estimator of g .

2.1 Relation Between h and h'

We wish develop an estimate, \hat{h} , of the tidally induced portion of the spring discharge, h , and then remove it from the total discharge, f . The result is an estimate, \hat{g} , of the non-tidal discharge, g :

$$\hat{g}(x_i) = f(x_i) - \hat{h}(x_i), \quad i = 1, 2, \dots, n. \quad (2)$$

We use Pearson's correlation coefficient ρ (see, for example, Johnson (2005)) to measure the relation between h and h' . This statistical measure quantifies the degree of relation between two samples. It's value always lies between -1 and 1 , with ± 1 implying a linear relation, and values near 0 implying no linear relation.

The correlation ρ of the two signals is given by

$$\rho(h', h) = \frac{\sum_{i=1}^n (h(x_i) - \mu_h)(h'(x_i) - \mu_{h'})}{(n-1)\sigma_h\sigma_{h'}} \quad (3)$$

where μ refers to the sample mean of a signal and σ is the sample standard deviation. We assume that h and h' have a large positive correlation. For tide and discharge, this is not unreasonable, see Loper et al. (2005).

We note that Pearson's correlation ρ is related to the coefficient of determination, R^2 , of simple linear regression. However, one may not simply regress discharge on tide to determine the relation between these two signals. Such a method assumes that the relation between the two is constant over the interval. This is not the case for our data, especially for the irregular storm periods.

To estimate h , we examine the projections of the observed f into different scale spaces provided by the discrete wavelet transform (DWT) of Mallat (1989) and the associated multiresolution analysis (MRA) spaces. We then examine and choose from these projections to form a subsignal of f that is maximally correlated with the known function h' .

2.2 Wavelets and Multiresolution Analysis

Wavelets are very efficient at function estimation and compression. They excel at spatial adaptivity, optimality in terms of error rates, and low computational cost. Usually,

wavelet analysis is performed through the use of thresholding of wavelet coefficients, such as the VisuShrink method of Donoho and Johnstone (1994) or block methods of Cai (1999) or Chicken and Cai (2005). There, a noisy signal is transformed into empirical wavelet coefficients by the DWT, these coefficients are denoised by comparison with a specified thresholding rule, and the underlying function is estimated by applying the inverse DWT to these denoised coefficients.

Wavelets are an orthogonal series representation for functions f whose squares are integrable:

$$\int f^2 < \infty.$$

We denote this space as $L_2(\mathbf{R})$. Let ϕ and ψ represent the father and mother wavelet functions, respectively. There are large families of choices for these two functions available for use, see Daubechies (1992). Here, we choose ϕ and ψ to come from the commonly used set of wavelets that are compactly supported and generate an orthonormal basis. Figure 1 depicts a father and mother wavelet With finite support length 7. Let ϕ_{jk} and ψ_{jk} be the translations and dilations of ϕ and ψ :

$$\begin{aligned}\phi_{jk}(x) &= 2^{j/2}\phi(2^jx - k), \\ \psi_{jk}(x) &= 2^{j/2}\psi(2^jx - k).\end{aligned}$$

Then for any fixed integer j_0 ,

$$\{\phi_{j_0k}, \psi_{jk} | j \geq j_0, k \text{ an integer} \}$$

is an orthonormal basis for $L_2(\mathbf{R})$. Let ξ_{j_0k} and θ_{jk} be the usual inner product of a function $f \in L_2(\mathbf{R})$ and the wavelet basis functions:

$$\begin{aligned}\xi_{j_0k} &= \langle f, \phi_{j_0k} \rangle, \\ \theta_{jk} &= \langle f, \psi_{jk} \rangle.\end{aligned}$$

Then f can be expressed as an infinite series

$$f(x) = \sum_k \xi_{j_0k} \phi_{j_0k}(x) + \sum_{j=j_0}^{\infty} \sum_k \theta_{jk} \psi_{jk}(x).$$

Since we do not know f , but merely have a discrete realization of it, we estimate these wavelet coefficients using the DWT. If f is represented as a vector of dyadic length $n = 2^J$ for some positive integer J , then the DWT will give us a total of n estimated coefficients ξ_{j_0k} and θ_{jk} over the indices $j = j_0, j_0 + 1, \dots, J - 1$ and for all appropriate k . The lowest level possible for j_0 is 0, but higher values may be chosen.

Wavelets have the useful property that they can simultaneously analyze a signal in both time and frequency. This is accomplished by the fact that the series representation for f above can be viewed as several series: one series involving the father wavelet at level j_0 , and one mother wavelet-based series for each $j \geq j_0$. The first series corresponds

to the smooth, or coarse, structure of f . The other series correspond with increasingly detailed, high-frequency parts of f . Changing the index (or resolution level) j allows us to zoom in on the detailed structure of f or zoom out onto the smooth part of f . This is referred to as the multiresolution property of wavelets.

Each of the series at a different resolution level j corresponds to a projection of f onto a subspace of $L_2(\mathbf{R})$. Let V_j be the space spanned by the ϕ_{jk} and W_j be the space spanned by the ψ_{jk} . For wavelets as constructed by Daubechies (1992), V_j is orthogonal to W_l for $l \geq j$. Additionally, there is a ladder structure to these subspaces. If $f(\cdot) \in V_j$, then $f(2\cdot) \in V_{j+1}$. This creates a ladder of spaces:

$$\cdots \subset V_{j-1} \subset V_j \subset V_{j+1} \subset \cdots \subset L_2(\mathbf{R})$$

with $\overline{\cup_j V_j} = L_2(\mathbf{R})$ and $\cap_j V_j = \{0\}$. For large j , then, V_j is an approximation of the space $L_2(\mathbf{R})$. Each space V_j is “closer” to $L_2(\mathbf{R})$ in that it contains functions of increasing complexity.

The mother wavelet ψ is constructed so that not only is V_j orthogonal to W_l for $l \geq j$, but

$$V_{j+1} = V_j \oplus W_j$$

Using this, we choose a large value $j = J$ and use V_J as the approximation of $L_2(\mathbf{R})$. Then

$$V_J = V_{j_0} \oplus W_{j_0} \oplus W_{j_0+1} \oplus \cdots \oplus W_{J-1} \quad (4)$$

Each space V_{j_0} and W_l in the above expression represents parts of an $L_2(\mathbf{R})$ function at different resolutions. The wavelet transform projects the function f into each of these spaces.

As an example, consider the function seen in Figure 2. This function displays features at varying scales: a smooth portion trending left to right, and some steep jumps. This signal is made of $n = 2^7$ points. Using the father and mother wavelets shown in Figure 1, and setting $j_0 = 4$ ($J = 7$), the projections of this function into MRA spaces corresponding to W_6, W_5, W_4 and V_4 are shown in Figure 3. The original function can be reconstructed by adding all the projections from j_0 to $J - 1$ together.

In usual wavelet analysis, the different projections are summed together after some modifications involving thresholding have been applied to the wavelet coefficients. This is typically done for the purpose of signal compression or denoising, see Chicken (2003, 2005). In this paper, we present a new method of thresholding that is based on the correlation (3) of two signals.

2.3 Correlation Thresholded Estimate

We introduce a new type of thresholding to estimate g in (1). Let θ_{jk} and ξ_{j_0k} be the wavelet coefficients of f obtained from the DWT. We assume that f is of length $n = 2^J$. If this is not the case, the signal may be extended left or right to the closest, larger dyadic integer (a common practice in wavelet applications). Alternatively, one may interpolate

the data smoothly to a dyadic integer. We choose the lowest level j_0 to be 0, so there are a total of $J + 1$ MRA projections available.

Using these wavelet coefficients, we iteratively threshold them in order to form a subsignal of f that is maximally correlated with the known function h' . This function is our estimate of h .

Our method is a forward searching algorithm that thresholds these coefficients. We begin with a coefficient map vector M_0 of length n where each component of the vector is associated with a particular wavelet coefficient. M_0 is our initial state, with all entries set to 0. The first step in the algorithm is to set each component of map M_0 to 1, one at a time. Let M_0^{jk} be the map M_0 that has been modified to have a 1 in the position corresponding to θ_{jk} or ξ_{jk} position. This is equivalent to thresholding the coefficients

$$\begin{aligned}\hat{\theta}_{jk} &= \theta_{jk} \cdot I(M_0^{jk} = 1), \\ \hat{\xi}_{jk} &= \xi_{jk} \cdot I(M_0^{jk} = 1),\end{aligned}$$

where I represents the indicator function. The inverse DWT (IDWT) uses these thresholded coefficients to construct a function f_0^{jk} . Note that all the f_0^{jk} reconstructions sum to the complete function f . Let M_1 be the map M_0^{jk} that maximizes the correlation ρ between h' and the f_0^{jk} :

$$M_1 = M_0^l,$$

where

$$l = \arg \max_{jk} \rho(h', f_0^{jk}).$$

M_1 is the map containing the position of the single wavelet coefficient that maximizes the correlation between h' and the function constructed from that single coefficient.

The algorithm proceeds iteratively in this fashion. Step i modifies the map M_{i-1} to M_{i-1}^{jk} by changing a single 0 component at a time to 1. Components set to 1 in a previous step are not modified, so this is a forward only algorithm. The algorithm only adds coefficients. We set M_i to be M_{i-1}^l , where

$$l = \arg \max_{jk} \rho(h', f_{i-1}^{jk}),$$

and the f_{i-1}^{jk} are reconstructed using the wavelet coefficients from map M_{i-1}^{jk} .

The algorithm terminates when one of two events occurs. The first is that all the coefficients are used in a map. This is the case where the entire function f is maximally correlated with h' . The second event is when the maximum correlation found at step i is not p percent larger than the maximum correlation found at step $i - 1$. Setting p to 0 will add a wavelet coefficient provided it increases in correlation of the reconstruction to h' .

The method looks only for increases in the correlation. However, given the assumption that h and h' are positively correlated, this will be a common event.

The threshold rule is then

$$\hat{\theta}_{jk} = \theta_{jk} \cdot I(M_i^{jk} = 1, \text{ for any } i \in \{1, 2, \dots, n\}). \quad (5)$$

and

$$\hat{\xi}_{jk} = \xi_{jk} \cdot I(M_i^{jk} = 1, \text{ for any } i \in \{1, 2, \dots, n\}).$$

This rule provides the maximally correlated subsignal of f with h' for the algorithm given. The estimate for h is then

$$\hat{h}(x) = \sum_k \hat{\xi}_{0k} \phi_{0k}(x) + \sum_{j=0}^{J-1} \sum_k \hat{\theta}_{jk} \psi_{jk}(x)$$

and is provided computationally by the IDWT.

It is possible to modify it to a backward step algorithm by starting with all the wavelet coefficients in the map M_0 and removing coefficients one at a time to maximize correlation. Also, we could use a forward-backward approach. At any step, we consider both adding a single component and removing a previous component. Since our results were very good with the forward step algorithm, we did not investigate these others.

A property of Pearson's correlation ρ is that adding a constant to either, or both, signals does not change the value of the correlation ρ . Therefore, the estimate \hat{h} is only within a constant of h . It is estimating $h+c$ for some unknown constant c . This constant may be of no importance. In Section 3, we show this is the case with tide and discharge. There, we may assume $c = 0$ and ignore it. If the constant is of importance, additional information must be used to estimate c .

This algorithm applies to situations where the functions h and h' are positively correlated. If they were negatively correlated, then the algorithm may be modified to choose a map that minimizes the correlation (toward -1).

This estimator may be applied whenever h and h' are strongly correlated (negatively or positively), and h need only be estimated to within an additive constant c .

3 Wakulla Spring Discharge Data

We apply our method to two sets of data, with each set consisting of the discharge (or more precisely the flow speed), f , measured by a flow meter (operated by Florida State University) in the main vent of Wakulla Springs and the tide, h , measured by a tide gauge (operated by the University of South Florida) at Shell Point, Florida. The first set (Figure 4) consists of the discharge and tide measured between August 15 and August 28 of 2004. Each of these data strings contains 1024 points, equally spaced over the interval. The tidal signal (due primarily to luni-solar forcing) is very regular and is mostly at a high frequency. The discharge shows behavior at the same frequency, but also at lower frequencies. The discharge signal lags the tide signal by 45 minutes (see Loper et al. (2005)) and this has been accounted for in the data shown. Additionally, there was some missing data in the discharge signal. This has been replaced by interpolating with a cubic spline function.

The second set (Figure 5) is measured at the same locations, but now covers a time frame where the tide shows behavior at multiple frequency-scales (due to both regular

luni-solar forcing and two hurricanes). The discharge data also exhibits behavior at this multiple frequency-scales, but shows other low-frequency behavior as well. Each of these two data strings contains 2048 equally spaced measurement points. As mentioned in Section 2, attempting to model the tidal influence in the discharge with regression methods would fail in this case since the relation between the two signals is not constant over this period. This is readily observed in Figure 5. Standard smoothing of the discharge would not accurately remove the tidal component of the discharge, either. Additionally, one can see that Fourier analysis would not be well-suited to analyze this data. Even for the hurricane-free period in Figure 4, the tidal signal is not strongly periodic. In both figures, note the difference in scale between the discharge and the tide.

Examination of the two discharge signals in Figures 4 and 5 reveals that there is an added level of stochastic variability not present in the tide. This excess variability, or noise, (very likely due to turbulent fluctuations in the flow) can safely be filtered out without affecting the accuracy of the estimator proposed in Section 2.

However, there is a question of how much of this noise to take out. Removing too much will affect the relation between tide and discharge, removing too little leaves noise in the discharge. To determine how much of this noise to filter, we use a variant of the estimator described in the previous section.

As can be seen in Figure 3, the different resolution spaces of the MRA contain functions of different frequencies. The spaces with large indices are more complex and detailed than those with smaller indices.

The short-time variation in the discharge signal is represented by the levels of the MRA having large indices. To filter out noise unrelated to the tide, we proceed as follows.

Starting with the level having the largest index, we reconstruct the discharge using only this level of wavelet coefficients. We then determine the correlation between this partial reconstruction and the entire tide signal. If the correlation is smaller than a specified value, we know that this level may safely be filtered out.

If the first level examined has a small correlation, we then look at the level having the second highest index. If the reconstruction of the discharge using only these highest two levels of the MRA has small correlation with tide, then we proceed to the next resolution level, and so on.

The cutoff value we used to filter the noise is 0.01. Therefore, any cumulative sum of high level MRA reconstructions that has correlation with tide of less than 0.01 (in absolute value) is filtered out of the signal.

This method is similar to the thresholding explained in Section 2. The main difference here is that we are examining coefficients not one at a time, but one resolution level at a time. Also, instead of looking for large correlations, we are looking for small correlations.

Applying this filter method to the two sets of data in Figures 4 and 5 results in the denoised signals in Figure 6. This filter process has the added benefit of reducing the complexity of the search algorithm from Section 3. Any levels that have been filtered

as noise now have the corresponding coefficients set to 0. Since the DWT places half of the coefficients at the highest level, one-fourth at the next highest level, and so on, this results in a very small set of coefficients to be considered for the threshold maps M .

We are now ready to use the correlation thresholded estimate proposed in Section 2. Using the noise-filtered discharge signals with p set to 0, we get the results shown in Figures 7 and 8.

In both cases, the tidal component is well-realized by the estimator. Since the first case is very regular, standard smoothing would have led to a reasonable separation, although it would require user input to specify the level of smoothing desired. Specifically, one would need to know what the frequency is that needs to be separated out. The correlation between the unmodified discharge and the tide is 0.213 for this regular case. After the correlation thresholding has been applied to the discharge, the correlation between tide and the tidal component of discharge has risen to 0.762. The correlation threshold estimator filtered out the first two levels of the discharge as noise unrelated to the tide. The DWT of this signal is of length 1024, so this corresponds to thresholding all but 256 of the DWT coefficients to 0 (75%). Of the remaining coefficients, the estimator thresholded 145 of them to 0 and used the other 111 to build the tidal component of discharge.

The second case is more interesting and challenging; during this period of time two hurricane passed near the area of Shell Point and Wakulla Springs. Hurricane Frances arrived early in the period from the south. Initially it caused a rapid drop in the tide, followed by a rapid increase. Hurricane Ivan's effect on the area was an increase in the tide. Both these events are clearly seen in the tide signal in Figure 5. In addition to these large magnitude fluctuations in the tide, there also the regular diurnal and semidiurnal tide events. A smoother could not pick these both up simultaneously.

For this second case, the initial correlation between tide and discharge was 0.605. After filtering the noise, there were only 128 of 2048 DWT coefficients remaining, and 57 of these were thresholded to 0 by the algorithm. The final correlation of the tide and discharge tidal component was 0.753.

Note that the tidal component of the discharge is not an estimate of the tide. We expect and desire that the tidal component is of different magnitude and shape than the tide. We are not interested in an estimate of the tide, but rather in what influence it has on the discharge. A particular change in tide does not have an exact match in the discharge, but a change in discharge that is associated with the change in tide.

Once these tidal components of the discharge have been identified, they are then subtracted from the discharge. The remainder is the discharge that is related to non-tidal influences (rain, base flow, etc.).

A special case of h arises with our application (tide and discharge) that simplifies the estimator described in Section 2 in terms of computational complexity. Suppose the functions h and g are known to reside at different scale-frequencies that can be represented by the MRA spaces of the DWT. See Figure 4, for example. There, the tidal signal h' shows behavior only on high frequency scale. The discharge signal also

shows this behavior, as well as features at lower frequency. Let us assume that all the high frequency behavior is in the tidal component h .

In such a case, we modify the threshold in (5). We consider entire resolution levels of coefficients simultaneously, not one coefficient at a time. The map M_0 is taken as before, but M_1^* is the map in which all the entries corresponding to the most detailed level of wavelet coefficients (W_{J-1}) are set to 1. The correlation between h' and f_1^* is measured, and we proceed to the next step. Here, we set the map M_2^* to be all the entries corresponding to W_{J-1} and W_{J-2} . The correlation with f_2^* and h' is found. If it is at least $p\%$ larger than the previous correlation, we accept M_2^* as the map and proceed to step 3. We stop when the added level of coefficients does not increase the correlation enough or we have used all $J + 1$ levels of coefficients.

This method of thresholding works if the functions h and h' exhibit behavior at different frequency-scales than g . Using this method, we obtain the results in Figure 9. This is comparable to Figure 7. This estimator uses 504 of the 1024 wavelet coefficients. The number is greater than before because we are keeping or losing entire levels of coefficients at a time, rather than considering them individually as was done before. The correlation attained by this method between the tide and the tidal component of discharge is 0.643, compared to 0.762 (recall that the initial correlation was 0.213). This decrease in the accuracy is a result of the additional coefficients. Some coefficients in this variant are being included not because they increase the correlation between the two signals, but because they belong to a resolution level that is deemed important in the overall reconstruction. So, the advantage in computational complexity must be weighed against the decrease in the correlation ρ .

In both cases of our examples, the constant c is assumed to be 0. This is not unreasonable for our data. The influence of the tide on the discharge merely adds or subtracts from the base flow already present. It does not have a constant influence on the discharge.

4 Remarks

Our method works very well at removing the influence of one signal from another as evidenced by the preceding section. In general, the more distinct the two signals are with respect to their frequency behavior, the better the method performs.

The variant method discussed above clearly points this out. There, we take advantage of the fact that for the non-hurricane period, the tidal influence clearly resides in a different frequency level than the remaining portion of the signal. In such cases, the correlation thresholding shows a marked difference when crossing the MRA boundary between the tidal influence signal and the remaining discharge signal.

Unlike previous estimators, our method also works for signals that exhibit irregular frequencies, not just regular frequencies. The algorithm is more complex than in the previous case, but we still obtain an accurate estimate of the tidal influence on the discharge.

Finally, we note again that the goal is not to estimate the tide from observing the discharge, but to remove the tides influence from the discharge. Our method provides us only with that portion of the target signal that is attributable to the tide, not the tide itself.

References

- CAI, T. (1999). Adaptive wavelet estimation: A block thresholding and oracle inequality approach. *Ann. Statist.* **27** 898–924.
- CHICKEN, E. (2003). Block thresholding and wavelet estimation for nonequispaced samples. *J. Statist. Plann. Inference* **116** 113–129.
- CHICKEN, E. (2005). Block-dependent thresholding in wavelet regression. *Journal of Nonparametric Statistics* **17** 467–491.
- CHICKEN, E. and CAI, T. (2005). Block thresholding for density estimation: local and global adaptivity. *Journal of Multivariate Analysis* **95** 76–106.
- DAUBECHIES, I. (1992). *Ten Lectures on Wavelets*. SIAM, Philadelphia.
- DONOHO, D. and JOHNSTONE, I. (1994). Ideal spatial adaptation via wavelet shrinkage. *Biometrika* **81** 425–455.
- GAN, T. (2001). Precipitation of Western Canada wavelet, scaling, and multifractal analysis and teleconnection to large-scale climate anomalies. In *Proceedings of 15th Hydrotechnical Specialty Conference*. Canadian Society of Civil Engineers.
- JOHNSON, R. (2005). *Probability and statistics for engineers*. Pearson Prentice Hall.
- LABAT, D., ABABOU, R. and MANGIN, A. (2000). Rainfall-runoff relations for karstic springs. Part II: continuous wavelet and discrete orthogonal multiresolution analyses. *Journal of Hydrology* **238** 149–178.
- LIM, Y. and LYE, L. (2004). Wavelet analysis of tide-affected low streamflows series. *Journal of Data Science* **2** 149–163.
- LOPER, D. E., WERNER, C. L., CHICKEN, E., DAVIES, G. and KINCAID, T. (2005). Coastal carbonate aquifer sensitivity to tides. *Eos Trans. Am. Geophys. Union* **86** 353–357.
- MALLAT, S. (1989). Multiresolution approximations and wavelet orthonormal bases of $L^2(\mathbb{R})$. *Trans. Amer. Math. Soc.* **315** 69–89.
- VIDAKOVIC, B. (1995). *Statistical Modeling by Wavelets*. John Wiley and Sons, New York.

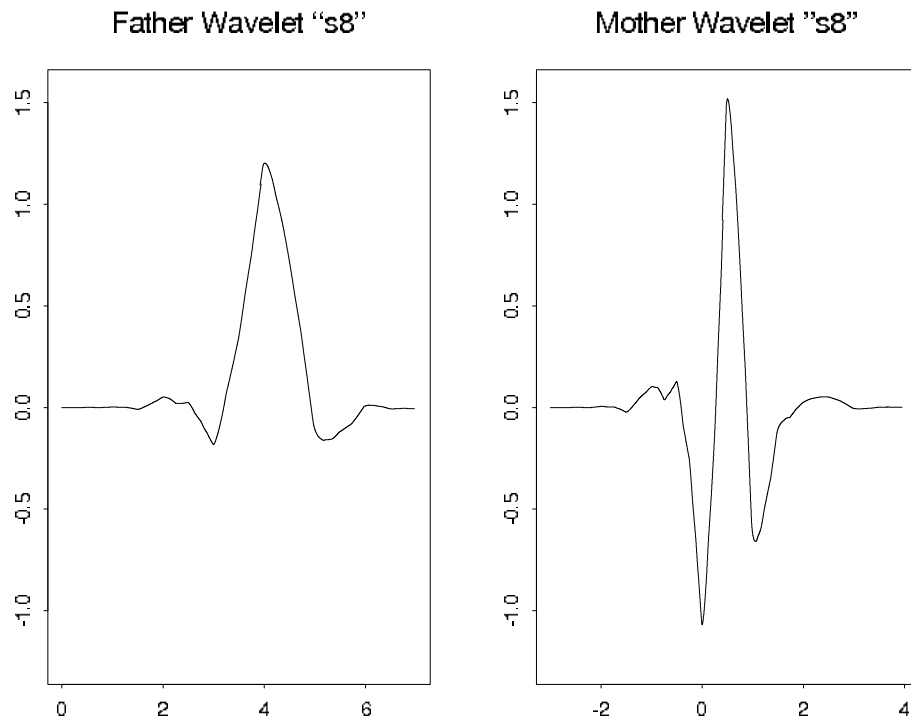


Figure 1: Example of father and mother wavelets functions ϕ and ψ .

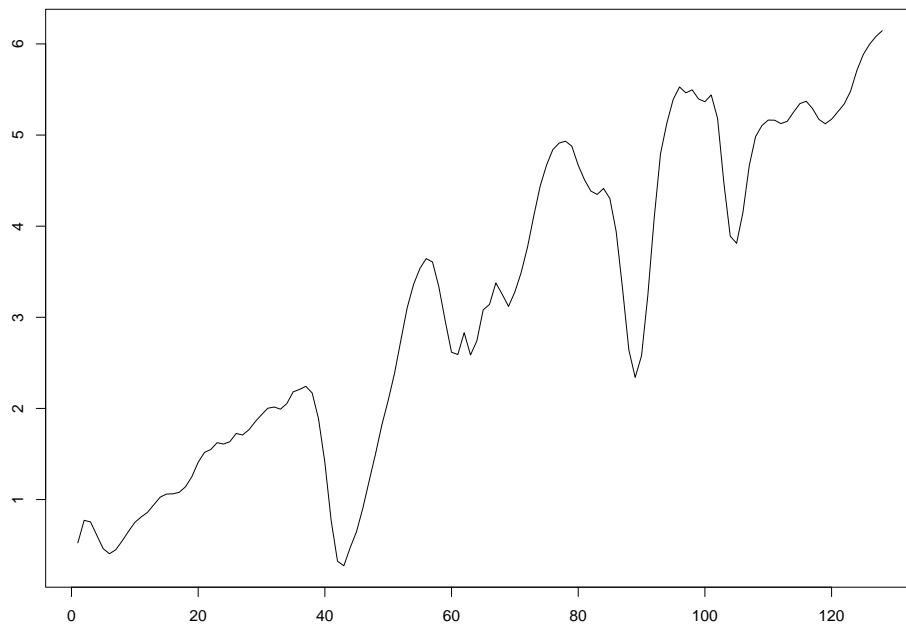


Figure 2: A function showing features at different scales.

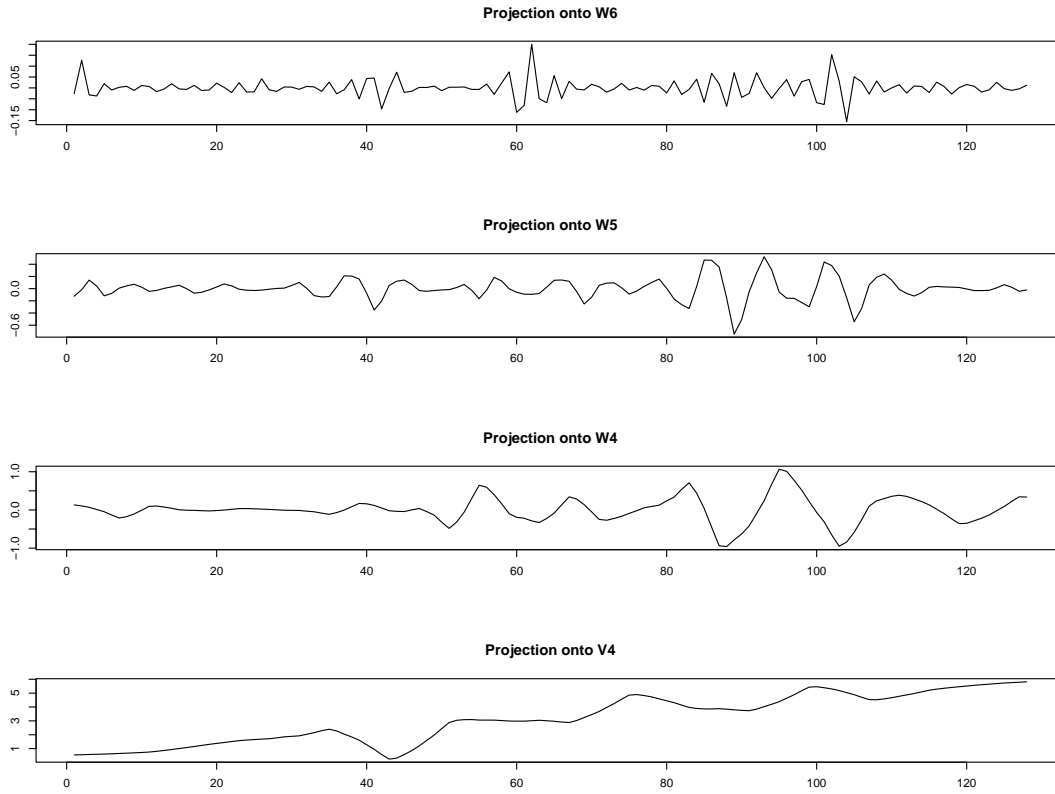
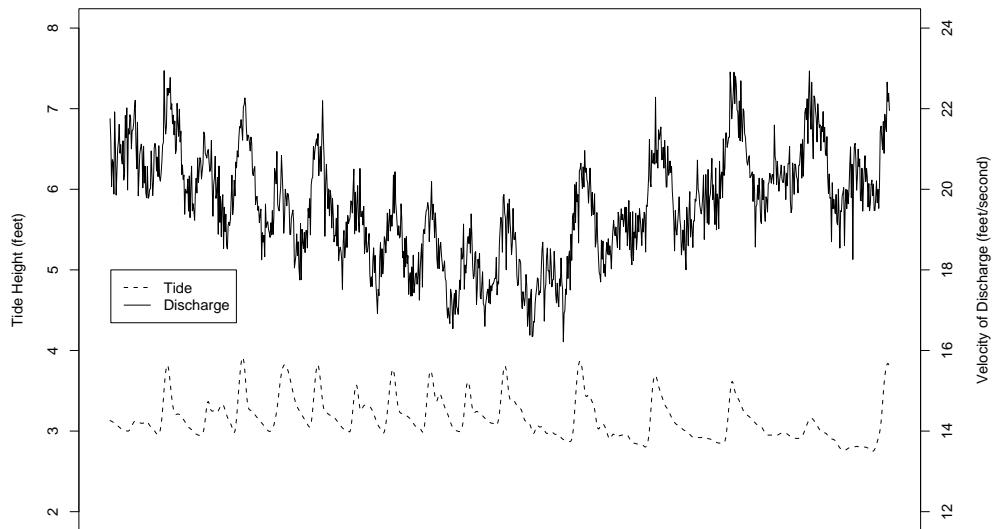


Figure 3: MRA of the function in Figure 2.



August 15, 2004 – August 28, 2004

Figure 4: Shell Point tide and Wakulla Spring discharge exhibiting regular behavior.

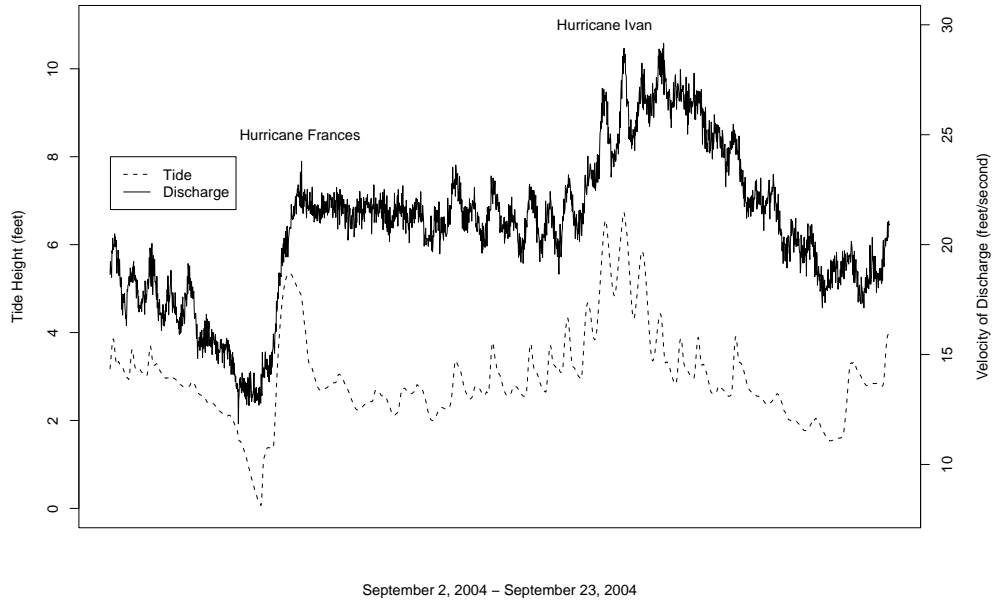


Figure 5: Shell Point, Florida, tide and Wakulla Spring discharge exhibiting irregular behavior due to storms.

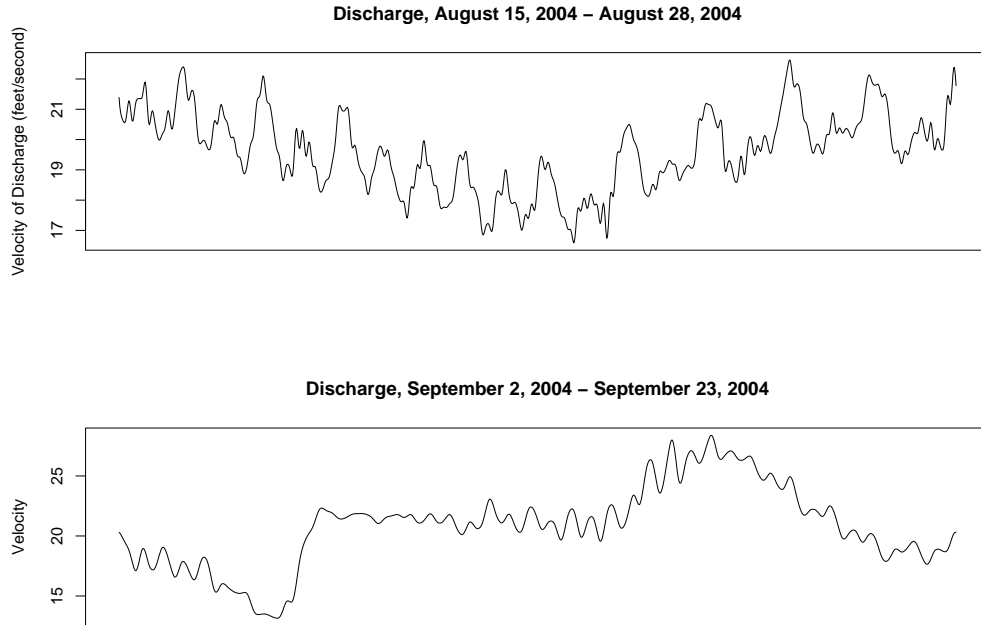
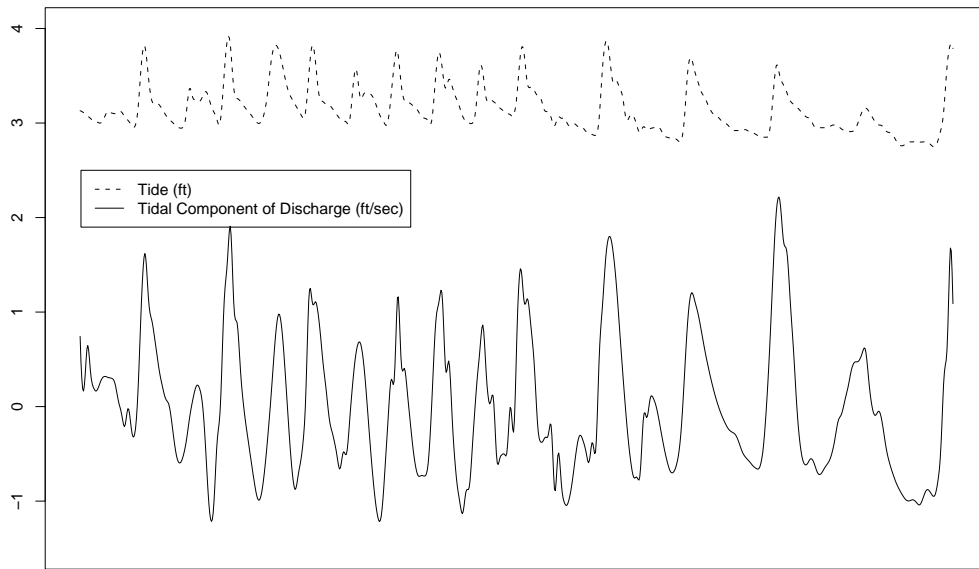
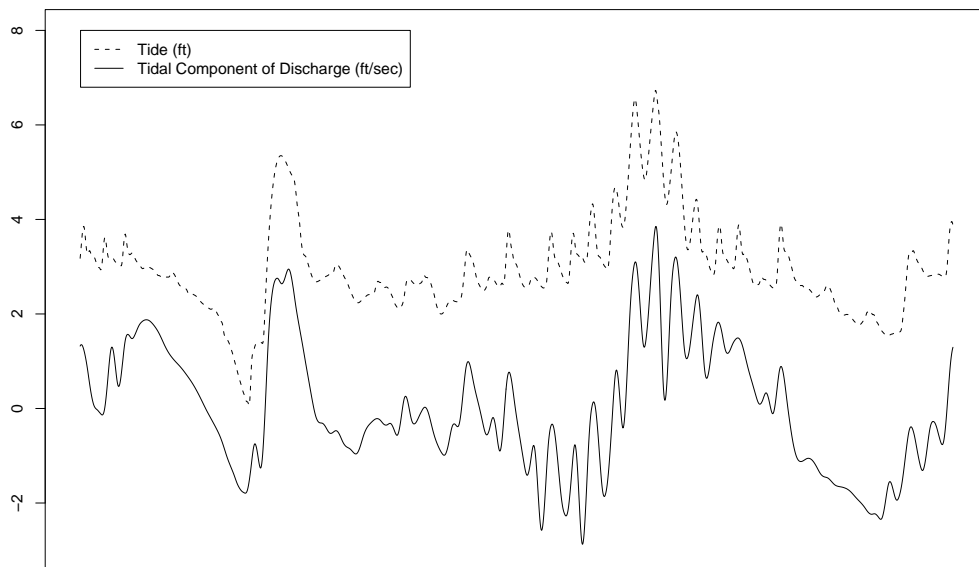


Figure 6: Discharge signals from Figures 4 and 5 with turbulence removed by correlation thresholding.



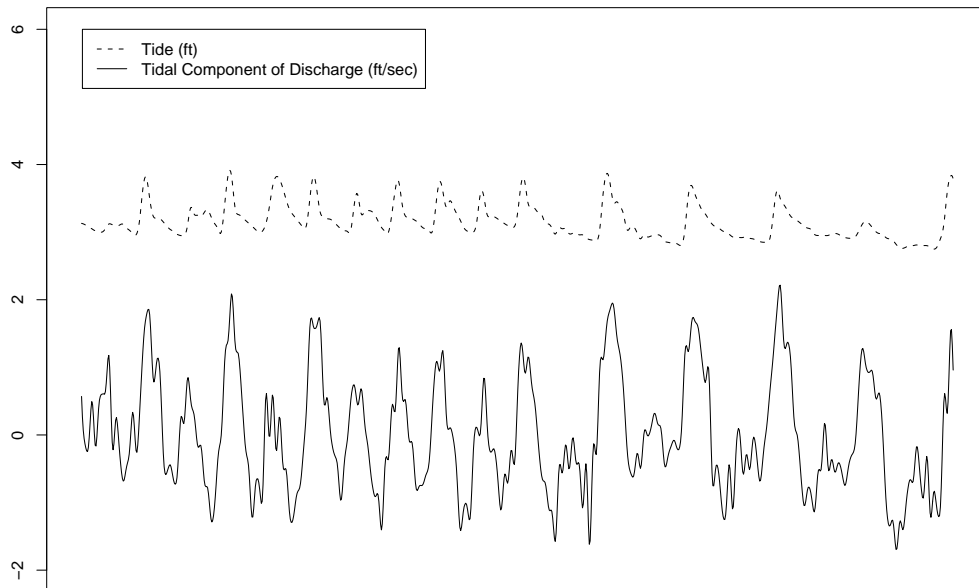
August 15, 2004 – August 28, 2004

Figure 7: The tidal component of the discharge signal.



September 2, 2004 – September 23, 2004

Figure 8: The tidal component of the discharge signal.



August 15, 2004 – August 28, 2004

Figure 9: The tidal component of the discharge signal using a variant of the correlation threshold estimator.